UNCLASSIFIED

Security Classification

AD 744773

DOCUMENT CONTROL DATA - R & D

(Security classification of title, body of abstract and indexing annotation must be entered when the overall report is classified)

1. ORIGINATING ACTIVITY (Corporate author)	2a. REPORT SECURITY CLASSIFICATION
Department of the Army Harry Diamond Laboratories Washington, D. C. 20438	UNCLASSIFIED
	2b. GROUP

3. REPORT TITLE

NUCLEAR ELECTROMAGNETIC PULSE SIMULATION BY DIPOLE ANTENNA ARRAY TECHNIQUES

4. DESCRIPTIVE NOTES (Type of report and inclusive dates)

Technical Report, 9 March 1971 through 30 November 1971

5. AUTHOR(S) (First name, middle initial, last name)

Janis Klebers, George D. Crowson

6. REPORT DATE	7a. TOTAL NO. OF PAGES	7b. NO. OF REFS
April 1972	38	3

8a. CONTRACT OR GRANT NO.	9a. ORIGINATOR'S REPORT NUMBER(S)
b. PROJECT NO. HDL E01EA USASAFCOM SW-S-53-70 c. AMCMS Code: 5910.21.63389 d. MIPR No. 1. 01182	HDL TM-72-9
	9b. OTHER REPORT NO(S) (Any other numbers that may be assigned this report)

10. DISTRIBUTION STATEMENT

Approved for public release; distribution unlimited.

11. SUPPLEMENTARY NOTES	12. SPONSORING MILITARY ACTIVITY
	USASAFSCOM P.O. Box 1500, West Station Huntsville, Alabama 35807

13. ABSTRACT

Time-domain dipole antenna array studies conducted at the Electromagnetic Effects Laboratory† of the Harry Diamond Laboratories for application to large scale nuclear electromagnetic pulse (EMP) simulation are described. Analytically and experimentally derived EMP environments for a single-dipole antenna are compared with corresponding data for multiple element broadside and collinear dipole antenna arrays. The multiple-element concept is studied as a technique for eliminating the need for extremely high voltages in the single element-type nuclear EMP simulators by substituting the superimposed electromagnetic fields radiated by several lower voltage sources to obtain the equivalent EMP environment. Experimentally measured input impedances are compared with the results from classical antenna theory to determine the effects of mutual coupling between elements in the array configurations. The aperture size of the array is shown to be an important factor in determining the pulse shape characteristics of the EMP environment, in the near and far fields. Results of the studies define specific advantages and limitations in the dipole antenna array techniques for nuclear EMP simulation.

†Formerly with USA Mobility Equipment R&D Center, Ft. Belvoir, Va. 22060

DD FORM 1 NOV 68 1473 REPLACES DD FORM 1473, 1 JAN 64, WHICH IS OBSOLETE FOR ARMY USE.

UNCLASSIFIED

Security Classification

A

14. KEY WORDS	LINK A		LINK B		LINK C	
	ROLE	WT	ROLE	WT	ROLE	WT
Dipole array	8	3				
EMF	8	3				
Pulsed antenna	8	3				
Dipole antenna	8	3				
Nuclear EMP simulation	8	3				

B

AD

MIPR 1.01182
AMCMS Code: 5910.21.63389
HDL Proj E01E4

HDL-TM-72-9

NUCLEAR ELECTROMAGNETIC PULSE SIMULATION BY DIPOLE ANTENNA ARRAY TECHNIQUES

by

Janis Klebers
George D. Crowson

Details of illustrations in this document may be better studied on microfiche

April 1972



U.S ARMY MATERIEL COMMAND
HARRY DIAMOND LABORATORIES
WASHINGTON, DC 20438

APPROVED FOR PUBLIC RELEASE DISTRIBUTION UNLIMITED

ABSTRACT

Time domain dipole antenna array studies conducted at the Electromagnetic Effects Laboratory† of the Harry Diamond Laboratories for application to large scale nuclear electromagnetic pulse (EMP) simulation are described. Analytically and experimentally derived EMP environments for a single dipole antenna are compared with corresponding data for multiple element broadside and collinear dipole antenna arrays. The multiple element concept is studied as a technique for eliminating the need for extremely high voltages in the single element type nuclear EMP simulators by substituting the superimposed electromagnetic fields radiated by several lower voltage sources to obtain the equivalent EMP environment. Experimentally measured input impedances are compared with the results from classical antenna theory to determine the effects of mutual coupling between elements in the array configurations. The aperture size of the array is shown to be an important factor in determining the pulse shape characteristics of the EMP environment in the near and far fields. Results of the studies define specific advantages and limitations in the dipole antenna array techniques for nuclear EMP simulation.

†Formerly with USA Mobility Equipment R&D Center, Ft. Belvoir, Va. 22060

Preceding page blank

CONTENTS

	Page
ABSTRACT	3
1. INTRODUCTION	7
2. SINGLE-DIPOLE ANTENNA	7
2.1 Time-Domain Expressions for the Electromagnetic Fields	9
2.2 Numerical and Experimental Results	10
2.3 Evaluation of Results	10
3. FIVE-ELEMENT BROADSIDE ARRAY	14
3.1 Superposition of Electromagnetic Fields	14
3.2 Time-Domain Expressions for the Electromagnetic Fields	17
3.3 Numerical and Experimental Results	18
3.4 Evaluation of Results	18
4. COLLINEAR DIPOLE ARRAY	21
5. EFFECTS OF MUTUAL COUPLING	28
5.1 Measurements of Antenna Input Impedance	28
5.2 Determination of Mutual Coupling Losses	30
6. EFFICIENCY FACTOR OF THE ARRAY MODELS	33
7. CONCLUSIONS	35
DISTRIBUTION	37

Preceding page blank

ILLUSTRATIONS

Figure		Page
1	Geometry for a typical antenna element and its image	8
2	Normalized input current pulse shape computed from equation (4)	9
3	The single-dipole antenna experimental configuration	11
4	A comparison of the theoretical and experimental results for the single dipole observed on the centerline at coordinates (x, y, z) = (40, 2, 0) ft	12
5	A comparison of the theoretical and experimental results from the single dipole observed off the centerline at coordinates (x, y, z) = (40, 2, 20) ft	13
6	Five-element broadside dipole array geometry	15
7	Five-element broadside array	16
8	A comparison of the theoretical and experimental results for the five-element broadside dipole array observed on the centerline at coordinates (x, y, z) = (40, 2 0) ft	19
9	Five-element broadside array environment measured off the centerline at (x, y, z) = (40, 2, 20) ft	20
10	Computed electric free field for a single- and five-dipole configuration	21
11	Collinear dipole array geometry	22
12	The collinear dipole array	23
13	A comparison of theoretical and experimental results for the collinear dipole array observed at point (C) in figure 11	24
14	A comparison of theoretical and experimental results for the collinear dipole array observed at point (F) in figure 11	25
15	A comparison of theoretical and experimental results for the collinear dipole array observed at point (D) in figure 11	26
16	A comparison of theoretical and measured results for the collinear dipole array observed at point (G) in figure 11	27
17	Time-domain reflectometry. Dipole antenna impedance as a function of height above the ground	29
18	Time-domain reflectometry. The effect of adjacent elements on the measured impedance of the dipole antenna	30
19	Network representation of mutual impedance	31

TABLES

I.a.	Comparison of measured and computed input impedance for a dipole antenna above a ground plane	31
b.	Comparison between computed and measured relative impedance change as a function of change in antenna height	31
II.	The array efficiency factor	34

1. INTRODUCTION

The RES (Radiating Electromagnetic Simulator) type antennas have been used successfully as nuclear electromagnetic pulse (EMP) simulators. These simulators are dipole antennas that are driven in the time domain by a MARX generator located at a biconical center feed section. A radiating dipole antenna is formed by extending cylindrical arms from the biconos. The major limitation of these types of simulators has been the relatively low voltages achieved to date for a single source pulser. The voltages have generally been less than 2 MV for operational dipole systems. A source in this range cannot meet the large area coverage requirements such as those that exist for the SAFEGUARD site. It is therefore necessary either to increase the voltage for a single source or to superimpose the electromagnetic environments of several sources to provide the required threat-level coverage.

Much work has been done in antenna theory on continuous wave (CW) dipole array systems. Such arrays have proved their usefulness in many applications. It is of interest, therefore, to examine the properties of these arrays for application to time-domain EMP simulation. In theory, one can go from a frequency domain to time domain by the Laplace or Fourier transformations. These are linear operations through which some of the useful properties of CW arrays can be expected to carry over to the time domain.

The work presented in this report was conducted at the Electromagnetic Effects Laboratory HDL. Whenever possible, theoretical results have been verified by experiment. Several time domain dipole arrays were studied in order to determine the possibility of application of such arrays to high field level nuclear EMP simulation.

2. THE SINGLE-DIPOLE ANTENNA

Consider first the single horizontal dipole antenna to establish a correlation between theoretical predictions of the radiated EMP environments and the experimental results obtained from the models studied in this report. The early time EMP fields of a single-dipole antenna can be predicted with the Hertzian dipole equations which, in the frequency domain, are given below.[1]

$$H_\phi(\omega) = A(\omega)\, e^{-jkr}\left(\frac{jk}{r} + \frac{1}{r^2}\right)\sin\theta \tag{1}$$

$$E_r(\omega) = A(\omega)\, e^{-jkr}\left(\frac{2z_0}{r^2} + \frac{2}{j\omega\epsilon r^3}\right)\cos\theta \tag{2}$$

$$E_\theta(\omega) = A(\omega)\, e^{-jkr}\left(\frac{j\omega\mu}{r} + \frac{z_0}{r^2} + \frac{1}{j\omega\epsilon r^3}\right)\sin\theta \tag{3}$$

where $A(\omega) = I(\omega)h/4\pi$, $I(\omega)$ is the antenna current, h = equivalent length of the antenna, $z_0 = \sqrt{\mu/\epsilon}$, $k = \omega\sqrt{\mu\ \epsilon}$, ω = rad/sec, μ and ϵ are the permeability and permittivity of free space,

[1] Ramo, S., Whinnery, J. R., Fields and Waves in Modern Radio. Second Edition, John Wiley & Sons, Inc., N.Y. 1964, p. 498.

respectively. The geometry for these and subsequently discussed components is shown in figure 1. The time domain expression for the antenna current I(t) is represented by:

$$I(t) = K\{(1 + \alpha_1 t)\, e^{-\alpha_1 t} - (1 + \alpha_2 t)\, e^{-\alpha_2 t}\} \tag{4}$$

where $K = h/4\pi$ determines the amplitude of the current, and α_1 and α_2, respectively, determine the fall and rise times of the current. A plot of I(t) is shown in figure 2. The value

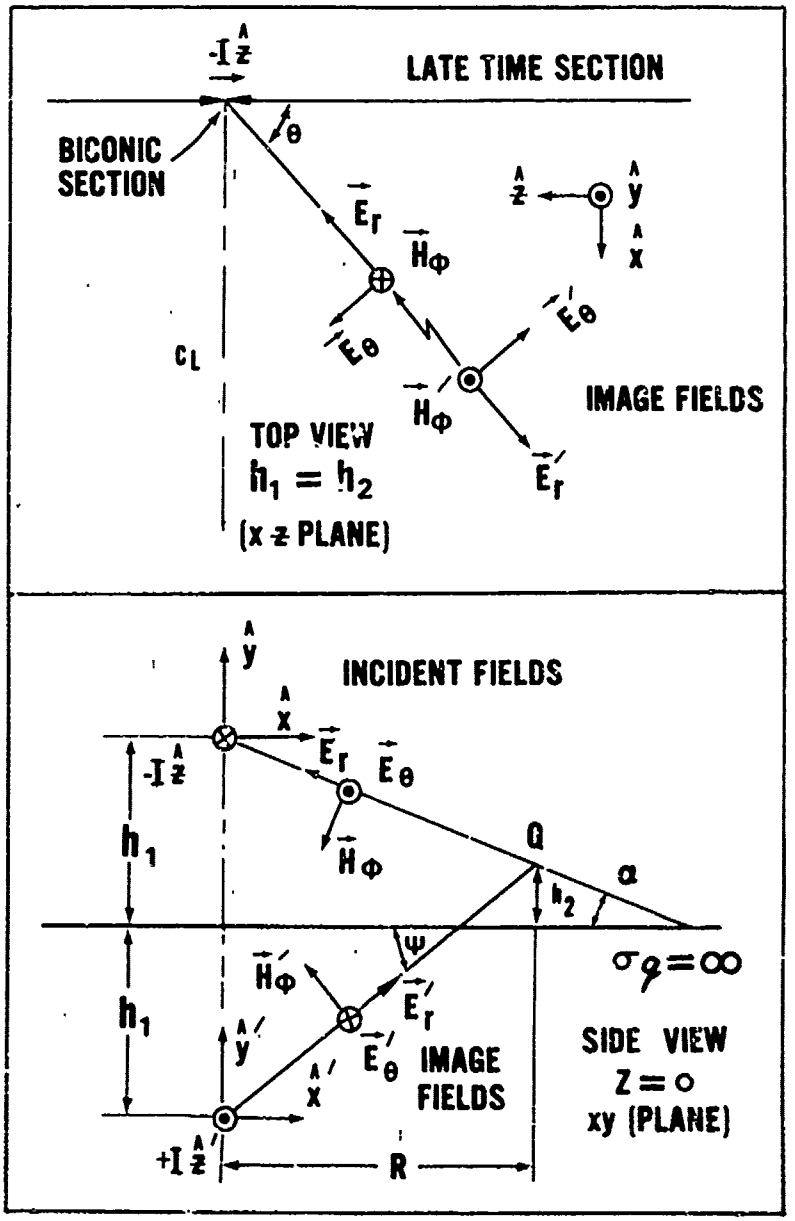


Figure 1. Geometry for a typical antenna element and its image.

$$\alpha_1 = 3\times10^4$$

$$\alpha_2 = 5\times10^8$$

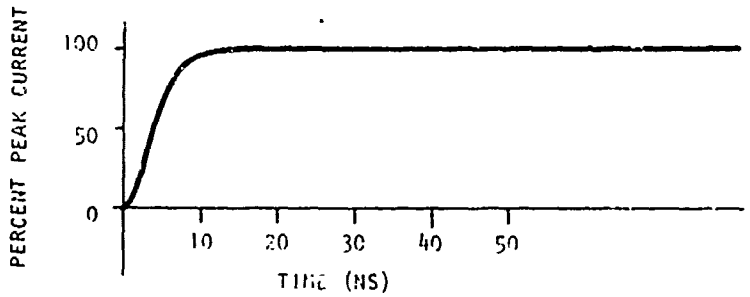


Figure 2. Normalized input current pulse shape computed from equation (4).

for the factor K is determined experimentally from either a direct current measurement on the antenna, or from a measurement of H_ϕ in the radiation field of the antenna.

2.1 Time-Domain Expressions for the Electromagnetic Fields

A time-domain solution for equations (1), (2), and (3) is obtained by the following procedure. The $j\omega$ variable is replaced by the Laplace variable $s = j\omega$ and the Laplace transformation is carried out. The results are convolved with equation (4) to obtain the time-domain expressions for the dipole fields:

$$H_\phi(t) = K\left(\frac{1}{r\,c}\frac{dI}{dt} + \frac{I}{r^2}\right)\sin\theta \tag{5}$$

$$E_r(t) = 2K\left(\frac{z_0 I}{r^2} + \frac{1}{\epsilon r^3}\int_0^t I\,dt\right)\cos\theta \tag{6}$$

$$E_\theta(t) = K\left(\frac{\mu}{r}\frac{dI}{dt} + \frac{1}{\epsilon r^3}\int_0^t I\,dt + \frac{z_0 I}{r^2}\right)\sin\theta \tag{7}$$

where $K = h/4\pi$ is assumed independent of frequency. This assumption requires that the dipole impedance remains constant over the pulse length of interest, and limits the solution to the early time regime. That is, a time $\leq (2h_1/c)$ in figure 1, where the dipole antenna does not receive ground reflections which affect impedance of the antenna. In all cases under study, the antennas are located at a height h_1 above the ground so that the rise time is less than the ground interaction time. We therefore expect a good representation of the peak fields from equations (5), (6), and (7).

Ground reflections in the radiation field alter the free-space waveshape and must be taken into consideration when comparing theoretical and measured results. In the high-frequency (early time) range, the ground acts as a good conductor and thus the theory of images can be applied by considering the ground as a perfectly conducting plane. The reflected (image) fields in the presence of the perfectly conducting ground plane have the same form as equations (5), (6), and (7) but arrive at the point Q with a time delay corresponding to the path length difference transit time p/c between the incident and image fields, where p is the path length difference and c is the velocity of propagation. Orientation of the incident and image fields in figure 1 assure that the boundary conditions are satisfied at the conductor surface ($h_2 = 0$). We also note that the Fresnel reflection coefficient assumes the correct limiting values of +1 and -1 for vertical (electric field parallel to plane of incidence, E_x, E_y) and horizontal (electrical field perpendicular to plane of incidence, E_z) polarizations, respectively.

The resultant fields in the presence of the ground plane are obtained by transforming equations (6), (7), and (8) from spherical to rectangular coordinates, and by combining the incident and image components with proper time delay and orientation. This procedure gives the x, y, z components of the EMP environment, which corresponds to the measured fields. The equations are given below, where the "prime" symbol denotes the image fields, and the subscript T represents the total, or resultant, field intensity.

$$H_T = (-H_\phi \sin\alpha - H'_\phi \sin\Psi)\,\hat{x} - (H_\phi \cos\alpha - H'_\phi \cos\Psi)\,\hat{y} \tag{8}$$

$$E_{xT} = (E_\theta \cos\alpha - E'_\theta \cos\Psi)\cos\phi - (E_r \cos\alpha - E'_r \cos\Psi)\sin\phi \tag{9}$$

$$E_{yT} = (E_r \sin\alpha + E'_r \sin\Psi)\sin\phi - (E_\theta \sin\alpha + E'_\theta \sin\Psi)\cos\phi \tag{10}$$

$$E_{zT} = (E_\theta - E'_\theta)\sin\theta + (E_r - E'_r)\cos\theta \tag{11}$$

2.2 Numerical and Experimental Results

Equations (8) through (11) have been programmed on a digital computer and numerical results have been obtained for comparison with the experimental results. The factor K in equation (4) has been determined experimentally from the radiated H_ϕ to be 38.42 amperes (A). Figure 3 shows the experimental configuration of the single-dipole antenna. A 30-kV power supply was used as the source to charge a pulser, which in turn fed a 30-ft cable section of 100-Ω impedance to the center section of the antenna. Three orthogonal components of the electric and three orthogonal components of the magnetic field were mapped at several ranges on and off the centerline (z = 0 plane) of the mapping area. Representative results are shown in figures 4 and 5, comparing the theoretically and experimentally derived field components. The curve marked with the z symbol in the magnetic field plots represents the free space incident field H_ϕ. The other plots correspond to the measured data shown in the oscilloscope pictures. The peak-measured field strengths are designated by each oscilloscope picture throughout this report.

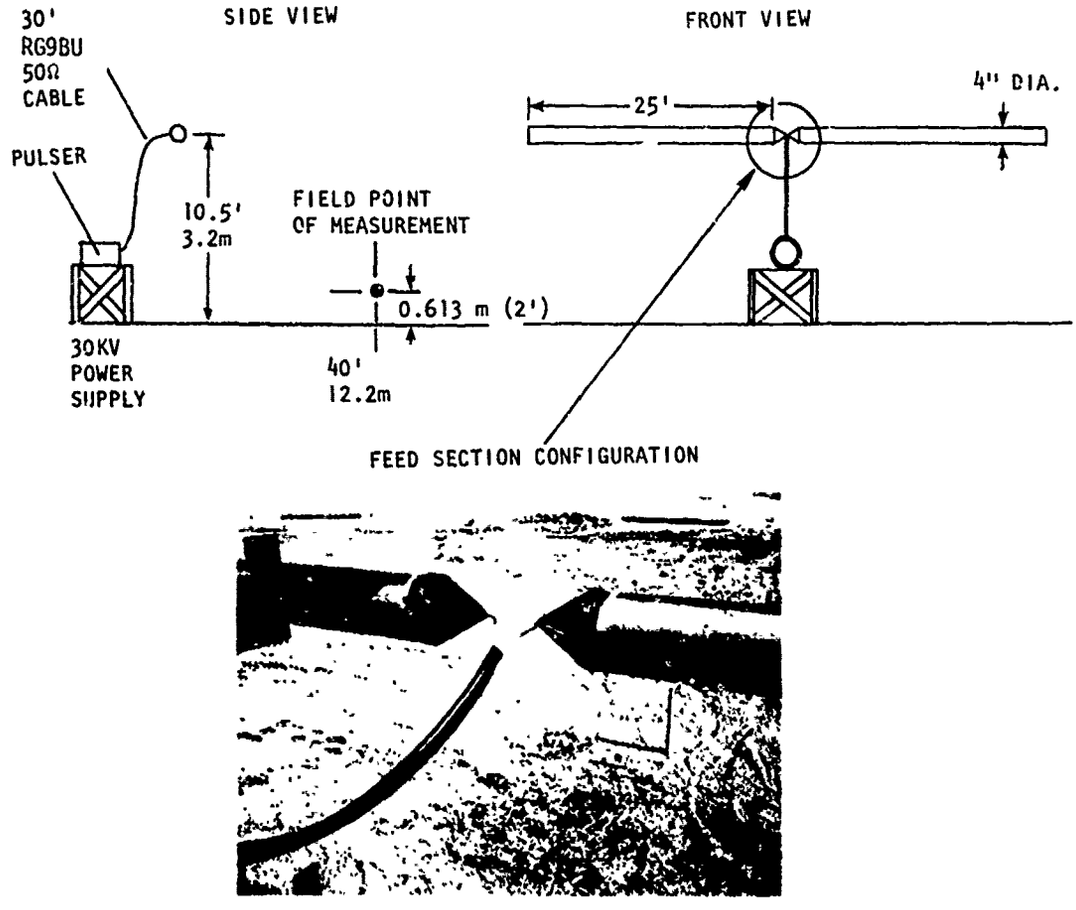
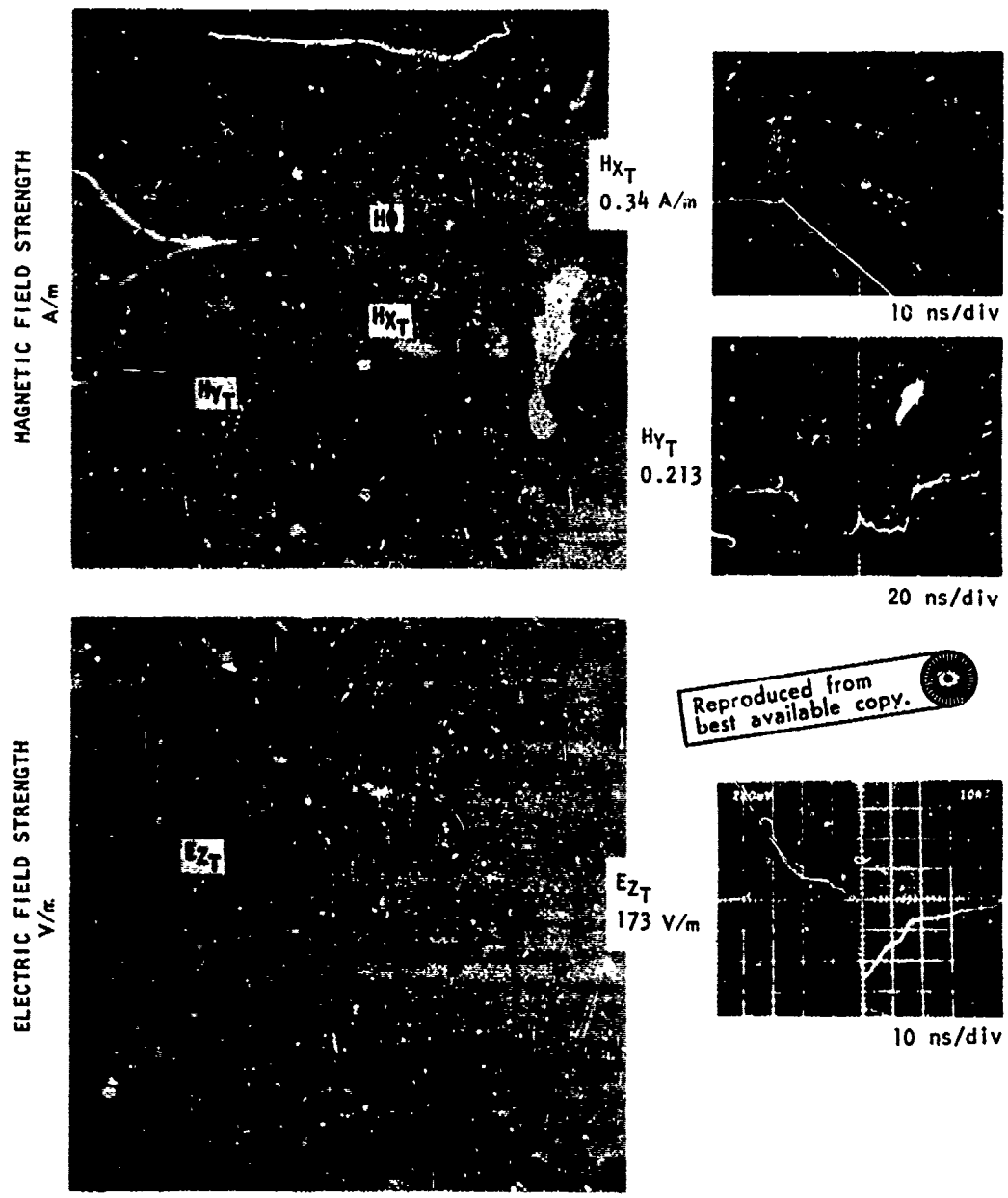


Figure 3. The single-dipole antenna experimental configuration.

2.3 Evaluation of Results

The components shown in figure 4 correspond to the TEM components of a plane wave. These are designated PRINCIPAL COMPONENTS. Off the centerline, the environment becomes nonplanar with the addition of the E_{xT} and the E_{yT} components. These components are not relatable to a horizontally polarized threat EMP and will be designated NON-PRINCIPAL COMPONENTS.

To correlate the simulator EMP environment with a particular threat EMP environment of interest, it is necessary to know the equivalent free field EMP environment radiated by the simulator. The EMP threat wave-shapes and amplitudes can then be directly compared with the simulator output. In general, the field-measurement sensors and the simulator itself are operated in the proximity of the ground. Because of this, the free-space environment cannot be measured directly. The theory of plane wave reflection at a smooth ground surface (or a perfectly conducting plane) can be used to obtain the free field from the measured tangential magnetic field (i.e., the magnetic-field component parallel to the ground surface). The tangential component of the incident magnetic field in figure 1 is the "x" component of H_ϕ. Boundary conditions require that the tangential component of H'_ϕ (the reflected field) be identical in sign to the tangential component of the incident field so that the tangential magnetic field will not vanish at the reflecting surface. At points above the surface, the two fields add



Reproduced from best available copy.

Figure 4. A comparison of the theoretical and experimental results for the single dipole observed on the centerline at coordinates (x, y, z)= (40, 2, 0) feet.

Reproduced from best available copy.

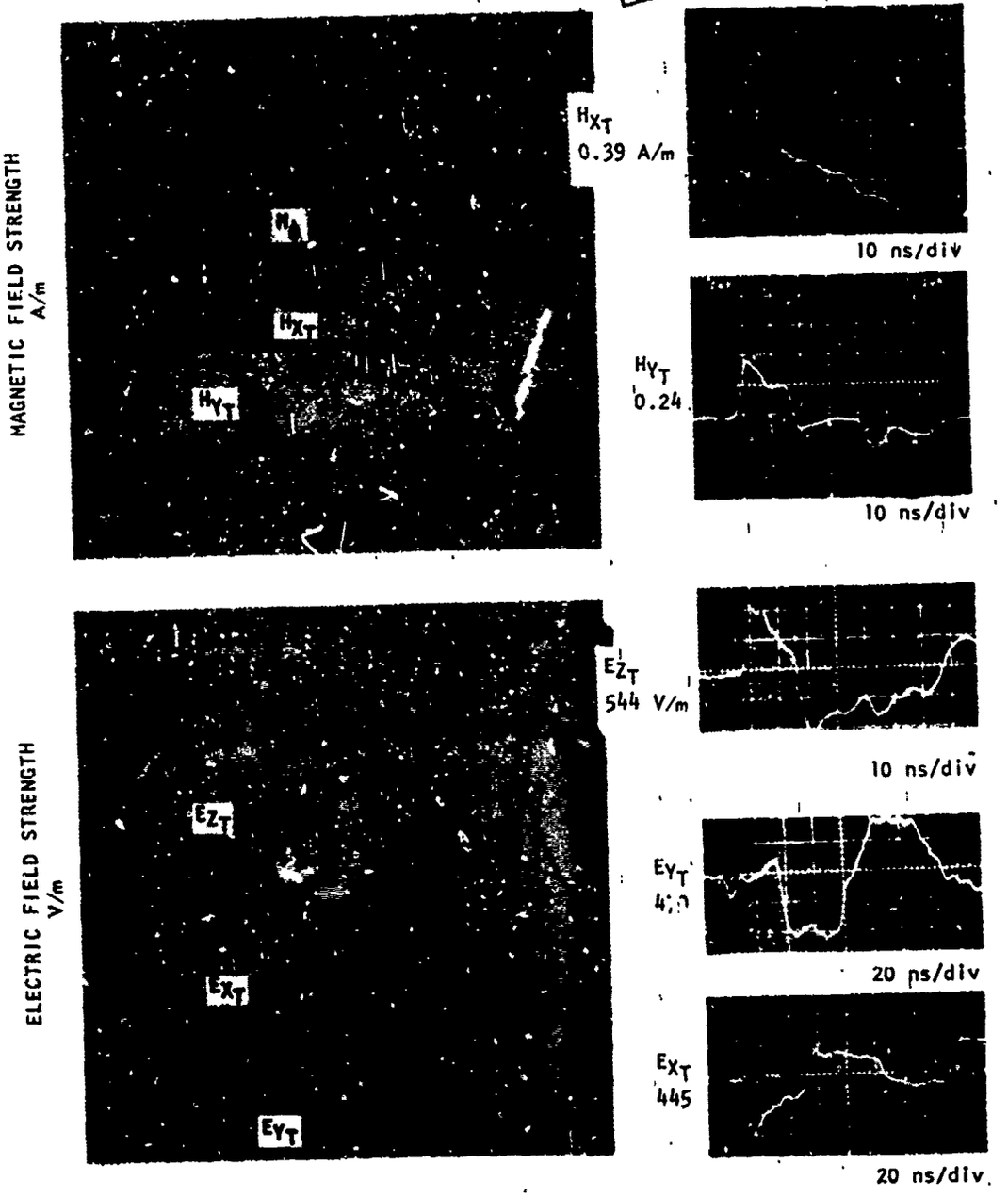


Figure 5. A comparison of the theoretical and experimental results for the single dipole observed off the centerline at coordinates (x, y, z) = (40, 2, 20) feet.

constructively (since both are of the same polarity) with a time shift equal to the path length difference transit time p/c between the incident and reflected fields. If the point of field measurement is close to the ground surface, p/c is less than the rise time of the free space incident pulse, and the resultant field H_{xT} preserves the waveshape of the incident free field. If such is the case, the incident and reflected tangential components add with very little time delay, and the only noticable difference in waveshape between the resultant field, H_{xT}, and the free field, H_{ϕ}, is a slight bump on the rising portion of H_{xT}. This can be verified in figure 4 by comparing the measured and computed waveforms of H_{xT} with H_{ϕ}. We also note that the magnitudes of the computed and measured values of H_{xT} agree closely, indicating that the assumption of perfect ground conductivity is justified in the early-time regime for the components that interfere constructively with ground reflections. The components that interfere destructively with the incident fields upon reflection are more sensitive to the infinite ground conductivity assumption, as evidenced by the smaller computed values of H_{yT} and E_{zT} compared with the measured results. These components vanish at the surface of a perfect conductor, but are greater than zero at the surface of an imperfect conductor, such as the earth. Hence, the measured values can be expected to be greater than the computed values near the surface of the ground. The same trends appear for measurements of H_{yT} and E_{zT} at a position off the centerline as shown in figure 5. The measured waveshape of H_{xT}, however, differs significantly off the centerline from the computed pulse shape, indicating a discrepancy between theory and experiment. The difference is due to radiation off the unterminated ends of the antenna used in the experiment, which is not included in the theoretical consideration. The additional radiation results from an abrupt current reversal at the end of each antenna arm, causing a magnetic field of opposite polarity to radiate which interacts with the principal magnetic field and changes the measured waveshape. The nonprincipal electric-field components agree well in pulse shape and amplitude. Therefore, for positions off the centerline, the theory is useful in predicting the relative amplitude of these components compared with the principal fields. The equations presented in this section have provided a method for predicting the EMP environment radiated by a pulsed-dipole antenna in the presence of the ground surface. The computations have been supported by experimental results. The subsequent sections of this report extend the methods developed for the single-dipole antenna to arrays of such antennas to determine their possible value as nuclear EMP simulators.

3. FIVE-ELEMENT BROADSIDE ARRAY

The field strengths produced by a single-dipole antenna nuclear EMP simulator are limited by the magnitude of the current and voltage that can be supplied to the antenna by a single-pulse source. This section considers a technique of increasing the simulated EMP environment by superimposing the fields of several simultaneously activated antennas which are distributed in an array to form a radiating aperture. The five-element broadside dipole array model was built to study this concept. Illustrations of the array are given in figures 6 and 7. The antennas are driven in parallel from the 30-kV source by five 30-ft-long 100-Ω cable connections. This configuration provides each antenna with a current equivalent to the single-dipole current discussed in section 2. As a result, the array aperture contains five times the amount of current compared to that of the single source.

3.1 Superposition of Electromagnetic Fields

The principle of superposition will be applied to compute the EMP environment radiated by the array. First, it is pointed out that although five times the single-source current exists in the array, the radiated environment is not necessarily assured to be five times as large. This is a consequence of two important factors.

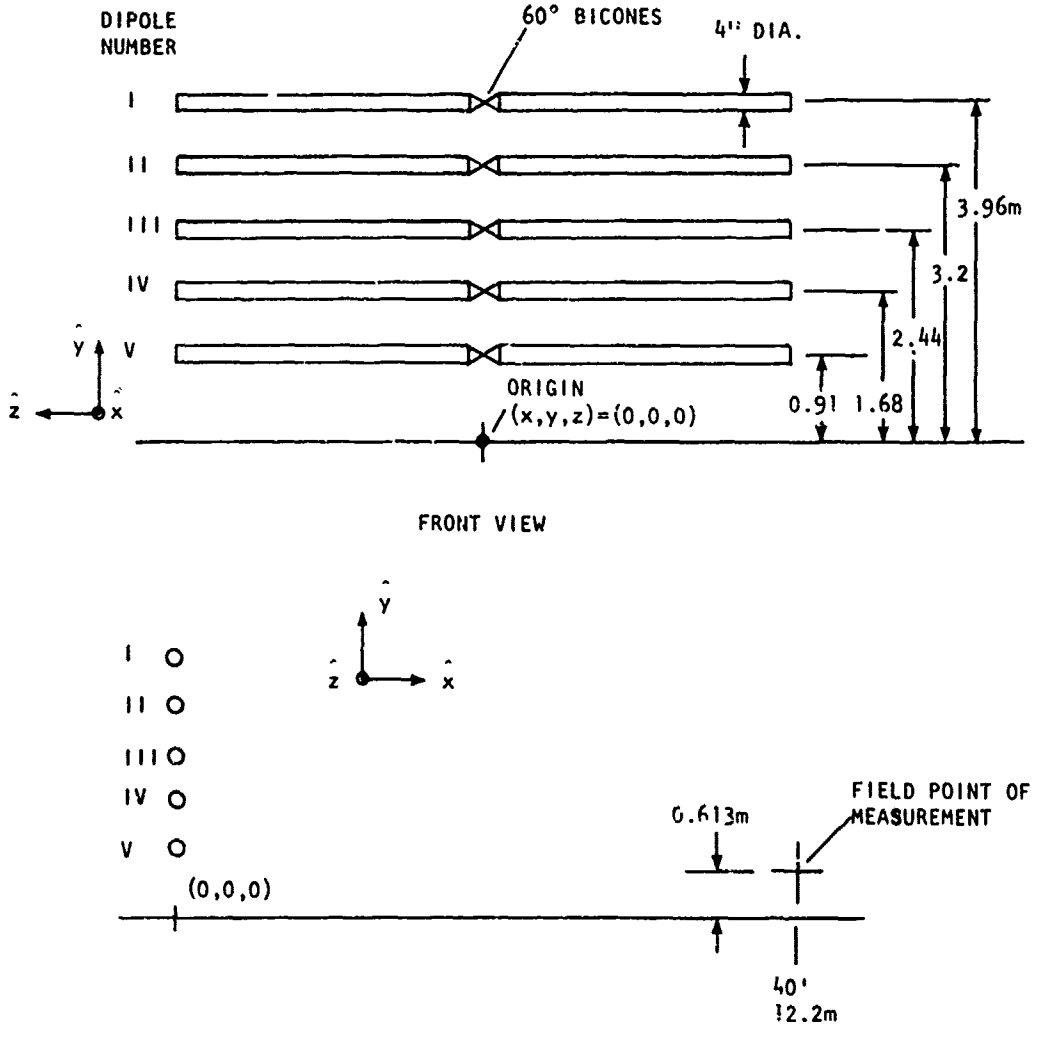
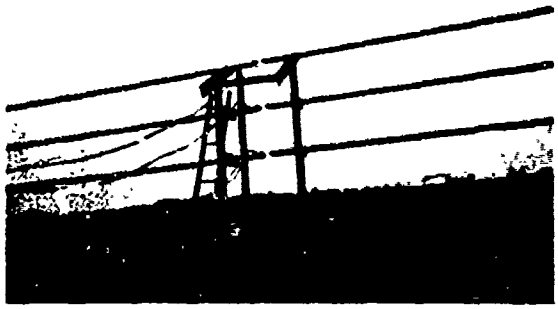
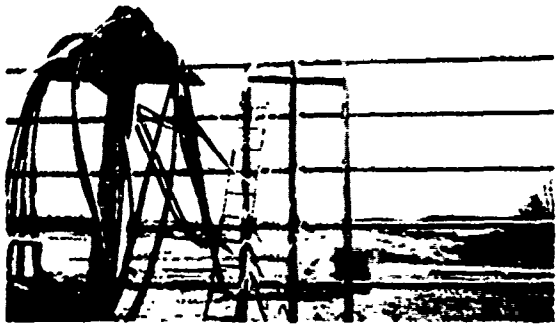


Figure 6. Five-element broadside dipole array geometry.

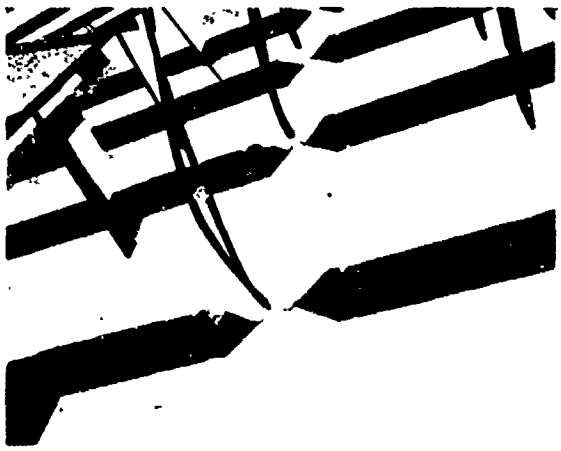
(1) The array is a distributed source, extending over several pulse risetimes in its dimensions. The fields computed at some distant observation point result from a retarded time superposition of the individual antenna environments. The retarded time refers to the different arrival time for the EMP wavefront from each source to the point of observation due to different path lengths between each antenna and the observation point. Thus, the addition of the fields from each source is spread out over a time equal to the maximum transit time difference between two extreme antennas of the array and the observation point. This results in a field magnitude smaller than that produced by a set of simultaneously superimposed pulses. Consequently, fields from the five-element array are expected to be less than five times that of a single source at finite ranges of observation. At an infinite distance of observation from the array, any finite aperture will appear as a point source and the retarded time effect will not be observed. However, for EMP applications, energy limitations preclude operation in the extreme far field of the array.



a. PARALLEL ARM CONFIGURATION



b. CABLE FEED FROM PULSER 30KV THRU 30 FT of RG9BU CABLE



c. CABLE FEED TO BICONE SECTIONS OF EACH ANTENNA

Figure 7. Five-element broadside array.

(2) The second important factor to consider is the possibility of losses occurring from mutual coupling between antenna elements. The radiating electric and magnetic fields of each antenna eventually strike every other antenna in the array, and some type of interaction (mutual coupling) must occur. From elementary electromagnetic theory, one expects the coupling to be in the form of induced currents which are smaller than, and tend to oppose, the initial source currents on the antennas. Thus, in addition to the retarded time effect, mutual coupling can be expected to further reduce the magnitude of the EMP environment radiated by an experimental array. As a starting point only the effects of retarded time superposition will be included in the array field equations, and the study of mutual coupling effects is considered in a later section of this report.

3.2 Time-Domain Expressions for the Electromagnetic Fields

Ideally, each antenna radiates the electromagnetic fields described by equations (5), (6), and (7). The equations corresponding to equations (8) through (11) for the single antenna are expressed for the array in terms of the retarded time summation over the number of antennas, N = 5, in the array:

$$H_{xT} = -\sum_{n=1}^{N} (H_{\phi n} \sin \alpha_n + H'_{\phi n} \sin \Psi_n) \tag{12}$$

$$H_{yT} = -\sum_{n=1}^{N} (H_{\phi n} \cos \alpha_n - H'_{\phi n} \cos \Psi_n) \tag{13}$$

$$E_{xT} = \sum_{n=1}^{N} \{[E_{\theta n} \cos \alpha_n - E'_{\theta n} \cos \Psi_n] \cos \theta_n - [E_{rn} \cos \alpha_n - E'_{rn} \cos \Psi_n] \sin \theta_n\} \tag{14}$$

$$E_{yT} = \sum_{n=1}^{N} \{[E_{rn} \sin \alpha_n + E'_{rn} \sin \Psi_n] \sin \theta_n - [E_{\theta n} \sin \alpha_n + E'_{\theta n} \sin \Psi_n] \cos \theta_n\} \tag{15}$$

$$E_{zT} = \sum_{n=1}^{N} \{(E_{\theta n} - E'_{\theta n}) \sin \theta_n + (E_{rn} - E'_{rn}) \cos \theta_n\} \tag{16}$$

where the "prime" symbol denotes the reflected (or image) field in each equation. The n subscripted field components contribute to the summations for the resultant fields only after the propagation time from the nth source of the point of observation Q has elapsed. Figure 1 shows the angles and field components for a typical element of the array. Equations (12) through (16) apply for any number N of mutually parallel dipole antennas which are located at arbitrary positions parallel to the ground surface. The nth field component, its corresponding retarded time, and the angle α_n, Ψ_n, and θ_n are computed by using the geometry illustrated for a typical source and observation point in figure 1. The equations have been programmed on a digital computer to provide numerical results.

3.3 Numerical and Experimental Results

Field measurements were conducted on the experimental model for comparison with the theory. A typical set of results is shown in figures 8 and 9 for the observation point at 40 ft on and off the centerline in the test area. As was the case for the single-dipole antenna, the computed H_ϕ plot represents the free space radiated magnetic field of the array. The T subscripted components correspond to the ground interacted fields (i.e., the incident free space plus the ground-reflected environments) which represent the measured fields shown in the oscilloscope pictures in figure 8. Again one observes that the measured tangential magnetic field H_{xT} compares closely in waveshape with thetheoretical H_{xT} and H_ϕ plots, and represents a reliable means of determining experimentally the free-space output of the source. In comparing magnitudes, the theoretical value for H_{xT} is greater than the measured value. This indicates that the omission of mutual coupling from the computations has affected the results. The reflection at 35 nsec corresponds to the mismatch at the unterminated ends of the antennas.

Figure 9 shows the measured environments off the centerline of the test area. In this region, the nonprincipal components are significant in magnitude, just as they were in the single antenna case, and the environment is nonplanar.

3.4 Evaluation of Results

A study of the computed electric free field indicates that the peak free field for the five-element array is approximately five times greater than the free field of the single antenna. Retarded time superposition has not affected the magnitudes appreciably for the particular array dimensions under study in this section. This becomes apparent when the path length difference transit time is computed between the extreme elements I and V in figure 6. The time difference is 1.2 nsec which is less than the 4 nsec 10 to 90% free field pulse rise time of each antenna. Consequently, the retarded time degradation occurs within a time span of 1.2 nsec and is beyond the resolution of the measurements. Figure 10 shows the computed peak electric free field magnitudes for the single- and five-element source as a function of range along the center line.

The extension of the single-dipole equations to a multiple source array by the method of superposition has proved to be a useful technique for prediction of the array environment. The computations have been supported by the measured data. The approach has demonstrated the amplitude degradation due to retarded time superposition; also, it has shown for the particular array dimensions under study in this section that the effect is beyond the sensitivity of the measurements. The discrepancies between the computed and measured data are therefore attributed mainly to the omission of mutual coupling losses from the computations. This argument is supported by the 27% higher computed value of H_{xT} over the measured value of the component in figure 8.

The theoretical and experimental approach has also shown that the free-field waveshape radiated by the array can be obtained by measuring the tangential component of the magnetic field, H_{xT}. This component interacts constructively with the ground and preserves the waveshape characteristics of the free field. The remaining principal components H_{yT} and E_{zT} interact destructively with the ground and therefore exhibit the sharp-spike waveform due to interference from the ground-reflected wave within a few nanoseconds after the wavefront arrival at the observation point.

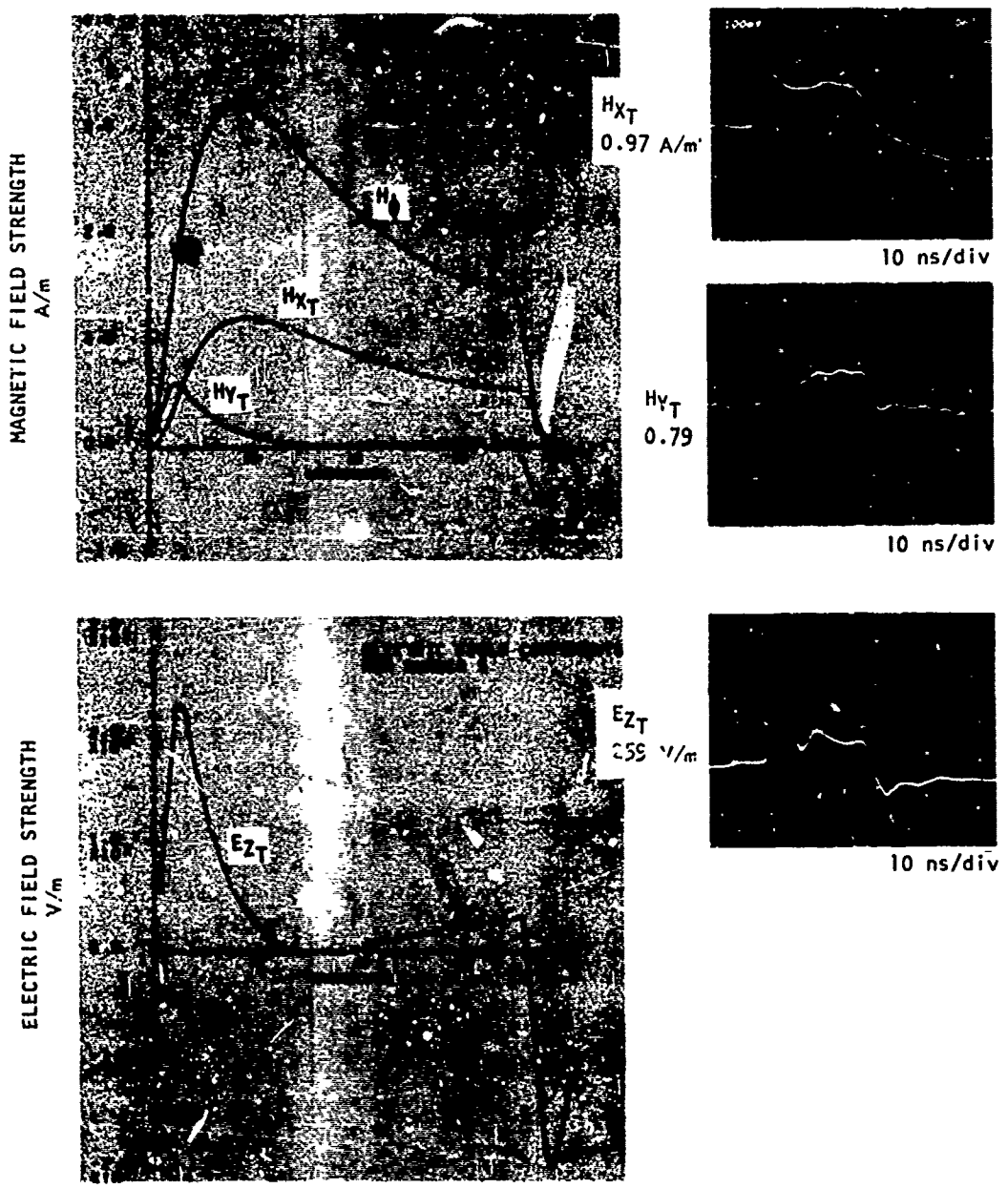


Figure 8. A comparison of the theoretical and experimental results for the five-element broadside dipole array observed on the centerline at coordinates (x, y, z) = (40, 2, 0) feet.

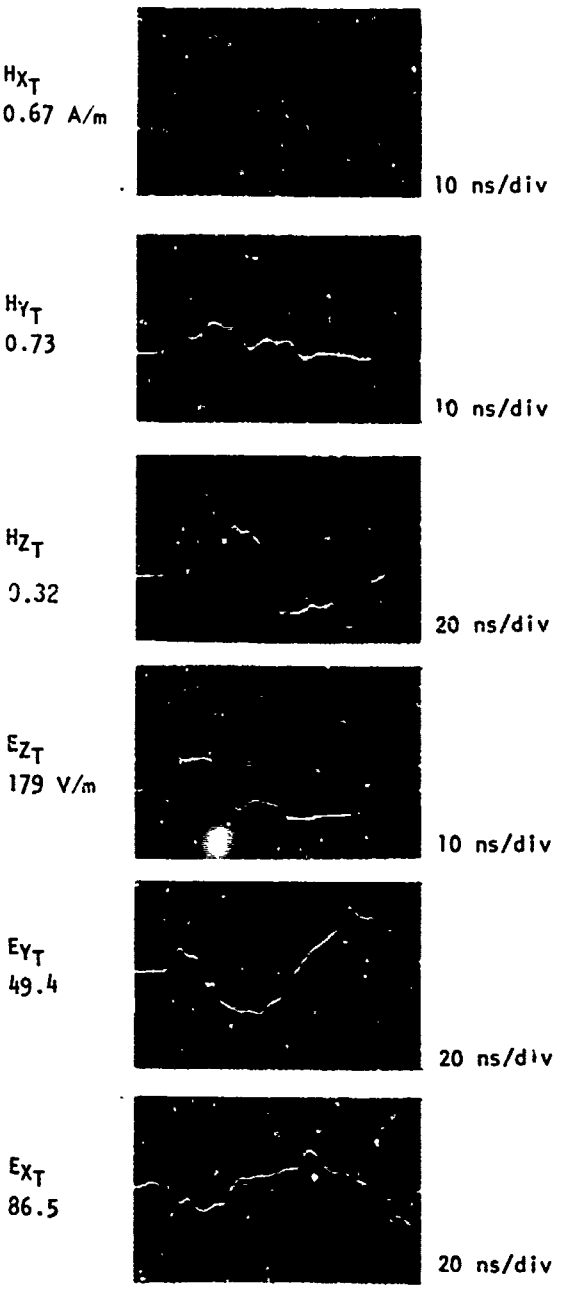


Figure 9 Five-element broadside array environment measured off the centerline at (x, y, z) = (40, 2, 20) feet.

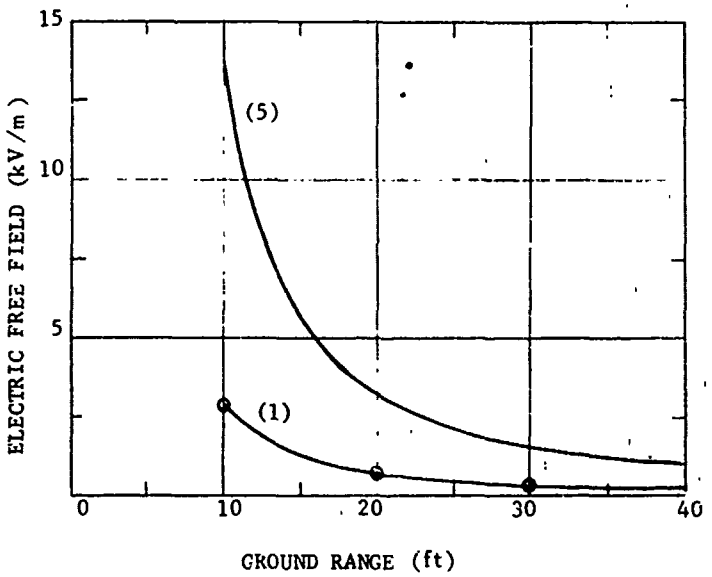


Figure 10. Computed electric free field for a single- and five-dipole configuration.

The results of the experimental and theoretical studies discussed in this section indicate that the array technique can indeed be used to increase field strengths radiated by EMP simulators. The basic limitations of this technique have been identified to be: (1) distributed source retarded time effects and (2) mutual coupling losses. These limitations warrant further study and are discussed in the remaining sections of this report.

4. COLLINEAR DIPOLE ARRAY

The collinear dipole array configuration shown in figures 11 and 12 was constructed to study the EMP environment of an array with a large aperture size compared to one rise time of a free-field pulse. Two collinear banks containing three antennas in each form the array. Each antenna has a current equivalent to the single-dipole current discussed in section 2. The z dimension is in the principal electric-field direction and corresponds to more than ten times the free field pulse rise time of a single element. In this case, the different arrival times of the wavefronts from antenna banks A and B are clearly visible in figures 13 and 14, which show data obtained at observation points C and F in the test area. The initial peak in the waveforms is due to fields arriving from antenna bank A. The second peak is due to the fields from antenna bank B which are displaced in time by a delay corresponding to the path length difference between the observation point and points A and B. The path lengths are given in figure 11. A comparison of transit time differences agrees closely with the computed and measured results in figures 13 and 14.

The field pattern of the collinear dipole array differs distinctly from the field patterns of the single dipole and the broadside array configurations. The polarity of the fields from each bank of dipoles in the collinear array is such that the nonprincipal field components (E_{xT}, E_{yT}, H_{zT}) tend to cancel and the principal field components (H_{xT}, H_{yT}, E_{zT}) tend to add constructively in the rectangular center region extending down range between A and B. Exact addition and cancellation of the principal and nonprincipal field components, respectively, occur only

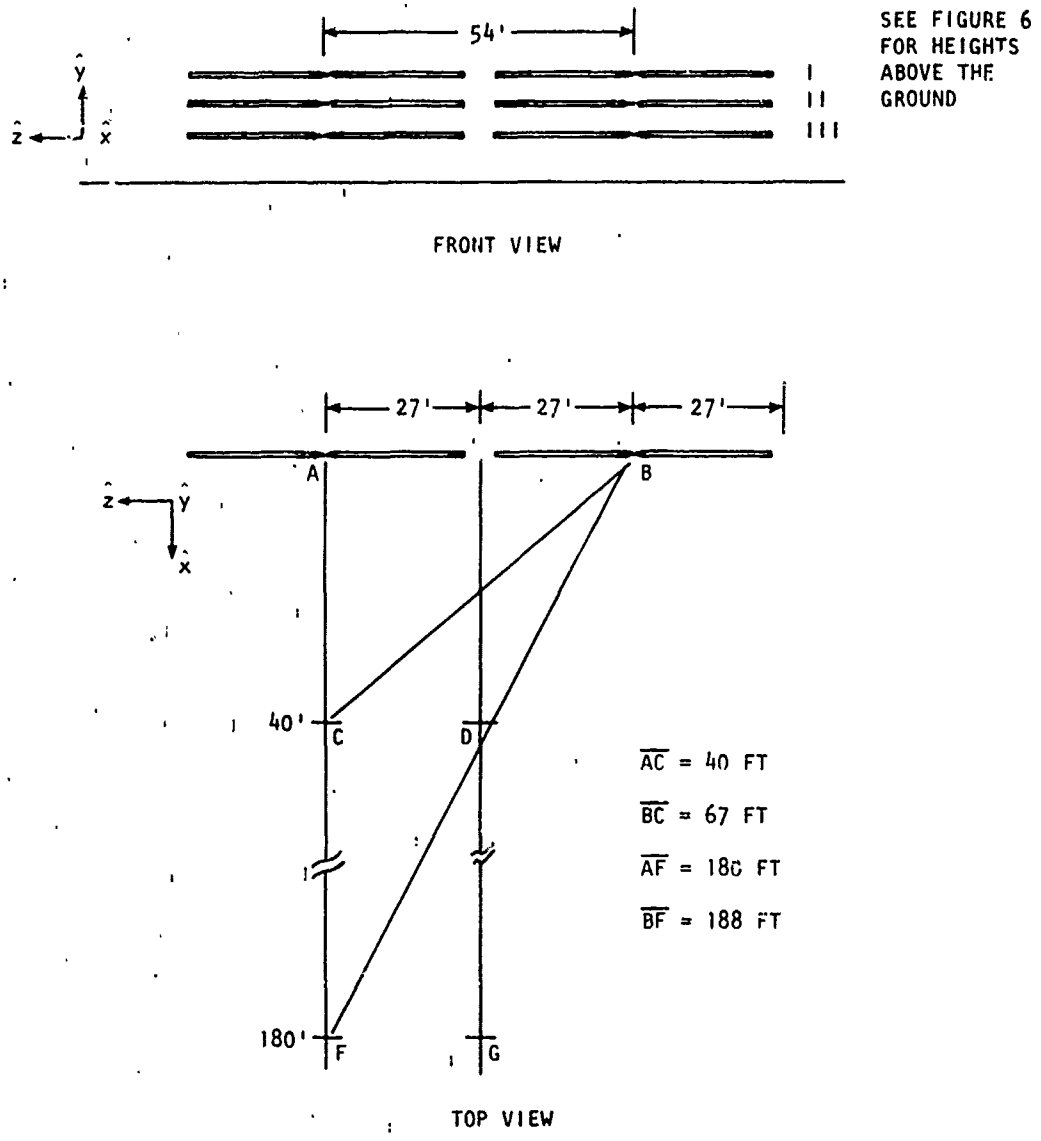


Figure 11. Collinear dipole array geometry.

on the centerline of the test area, defined along the line DG in figure 11. At other points in the rectangular center region, the largest contributions to the EMP environment from each antenna bank are due to the θ independent H_{xT} and H_{yT} given by equations (12) and (13), and to the dominant sin θ terms in equation (16). These terms have identical polarity for all antennas in the array and therefore add constructively in the field-equation summations. Because of this behavior, the collinear array has the desired characteristic of reinforcing principal field components and reducing nonprincipal field components within the center region. Ideally, this should increase the area of coverage by the principal fields compared with the coverage by the single dipole and the broadside array. The results, however, show that the gains in this respect are relatively small for the array dimensions under study.



a. ANTENNA CONFIGURATION

Reproduced from best available copy.

b. CABLE FEED FROM PULSER 30KV THRU 50 FT. OF RG9BU CABLE



c. CABLE FEED TO BICONE SECTIONS OF THE ANTENNAS

Figure 12. The collinear dipole array.

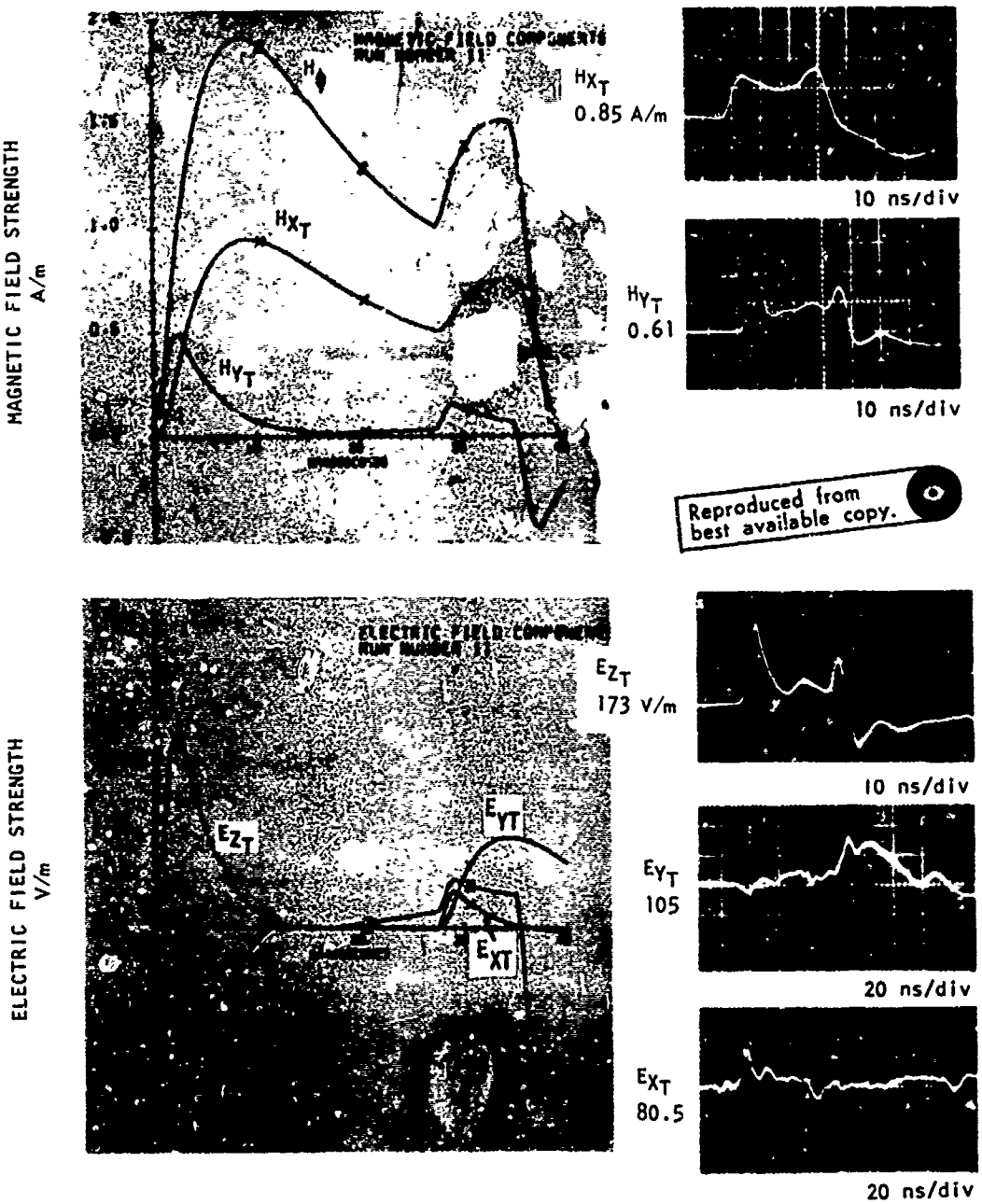


Figure 13. A comparison of theoretical and experimental results for the collinear dipole array observed at point (C) in Figure 11.

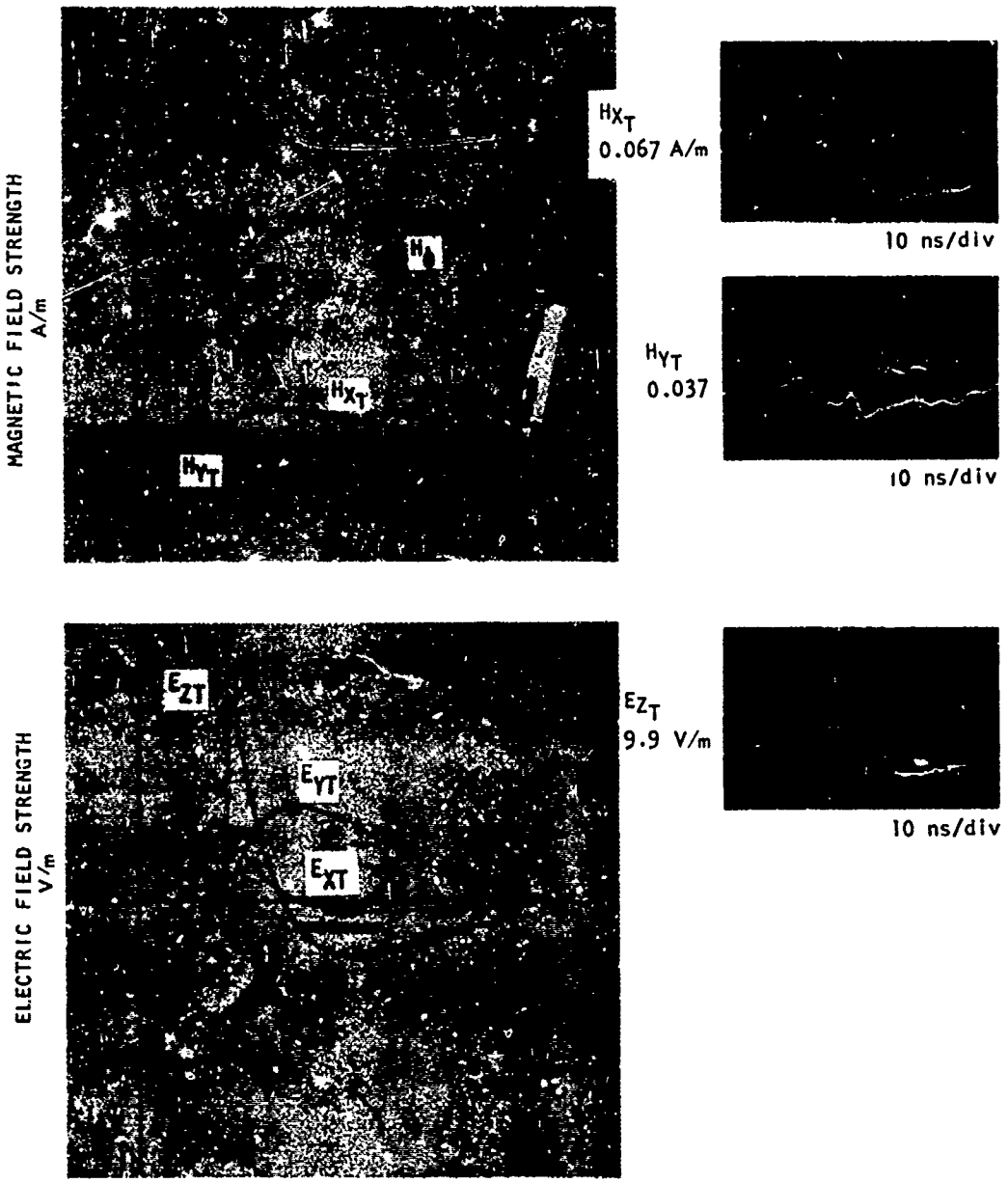


Figure 14. A comparison of theoretical and experimental results for the collinear dipole array observed at point (F) in Figure 11.

Reproduced from best available copy.

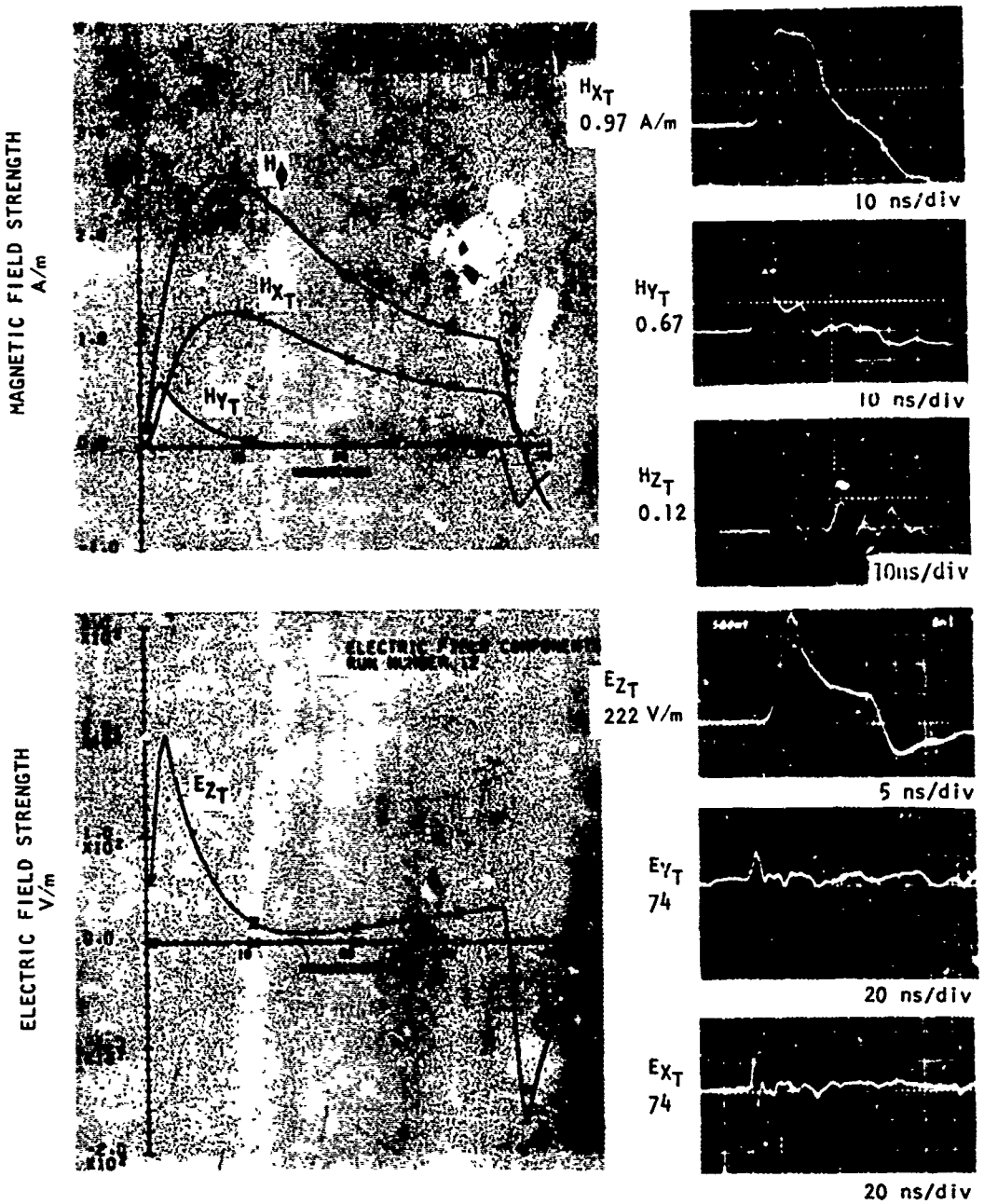


Figure 15. A comparison of theoretical and experimental results for the collinear dipole array observed at point (D) in Figure 11.

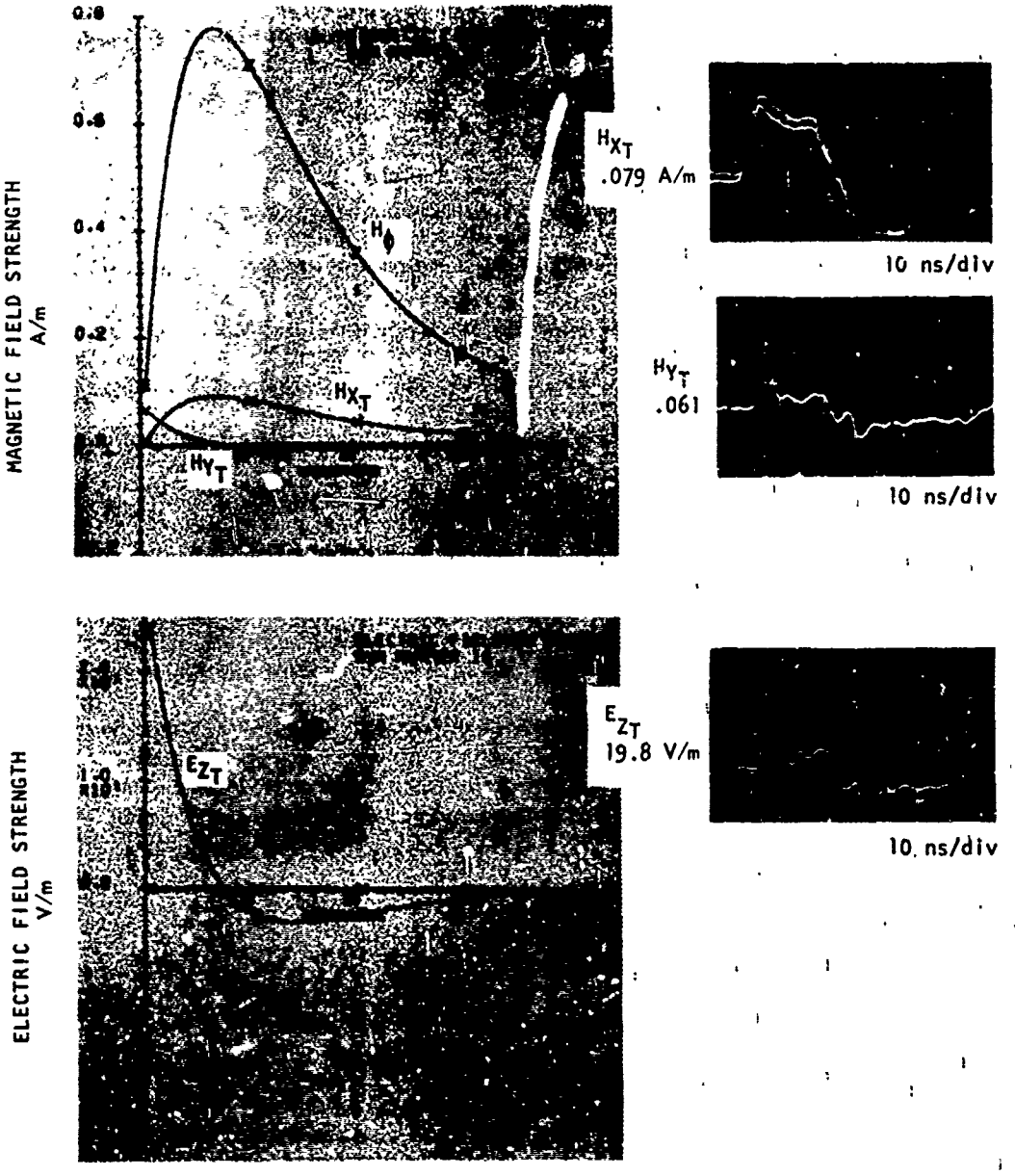


Figure 16. A comparison of theoretical and measured results for the collinear dipole array observed at point (G) in Figure 11.

The greatest limitation of the collinear array is the large time difference of wavefront arrival from the two antenna banks, which produce the two spikes in the waveforms. To eliminate this effect, the range of observation must be increased to a point where transit-time differences are less than one rise time of the free-field pulse from one antenna. Data in figures 13 and 14 illustrate the decrease in transit-time differences between the 40- and the 180-ft ranges. Even at the far range, the waveshape degradation has not been eliminated. Points F and G would have to be at least 700 ft away from the array to absorb retarded time effects within a single-element pulse rise time at positions between F and G.

5. EFFECTS OF MUTUAL COUPLING

The previous sections predict the dipole-array environments under ideal lossless conditions. The approach was successful in providing early time waveshape characteristics and relative amplitudes of the EMP fields. One would expect that the lossless case provides an upper bound to the performance of a dipole array. It is of interest, however, to know the extent of losses caused by mutual coupling between array elements. Such information would lend more confidence in equations (12) through (16) for use in the design of larger array systems. The lossless case would give an upper bound to the environment, and the extent of mutual coupling would provide an efficiency factor for the design.

5.1 Measurements of Antenna Input Impedance

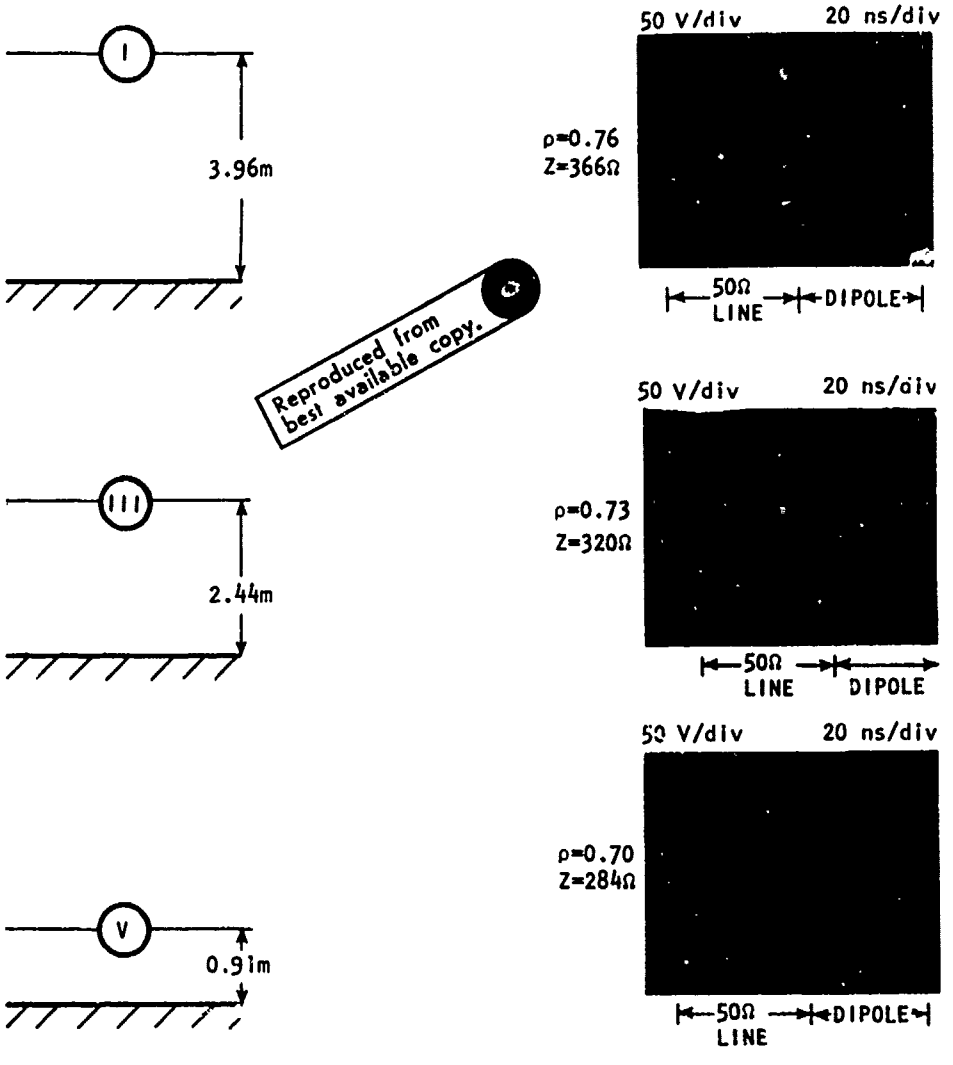
The network representation of mutual coupling between antennas will be used in this study. The approach is based on the knowledge of self and mutual impedance associated with the antennas. The antenna input impedance Z is measured by time-domain reflectometry (TDR). Figure 17 shows the measured input impedances for antenna elements I, III, and V of the broadside array. In each case, the other four antennas were removed for the measurements. The procedure used to make the measurement was to transmit a step-function input pulse through a 50-Ω reference cable to the antenna, and to observe the relative magnitude of the reflection (due to impedance mismatch) on a Tektronix 7704 oscilloscope. Standard TDR procedure is used to compute first the reflection coefficient ρ at the junction of the reference cable and the dipole antenna, and then to obtain the antenna input impedance Z from:

$$Z = R\left(\frac{1+\rho}{1-\rho}\right) \text{ ohms} \qquad (17)$$

where R is the reference 50-Ω impedance and the value of ρ is given next to each oscilloscope picture in figures 17 and 18.

Figure 17 shows the measured dipole antenna impedance as a function of antenna height above the ground. These measurements were taken to test the sensitivity of the TDR technique. The results show that the input impedance Z increases as the antenna height above the ground is increased. This trend is correct if the antenna and its image in the ground are considered as a two-wire transmission line with characteristic impedance Z_0 given by [1]

[1] Ramo, S., Whinnery, J. R., Fields and Waves in Modern Radio. Second Edition, John Wiley & Sons, Inc., N.Y. 1964, p. 364.



Reproduced from best available copy.

Figure 17. Time-domain reflectometry. Dipole antenna impedance as a function of height above the ground.

$$Z_0 = 120 \cosh^{-1}\left(\frac{s}{d}\right). \tag{18}$$

where d is the diameter of the two conductors and s is the separation distance. This equation applies for a line separated with an air dielectric and gives two times the impedance value for the antenna above a lossy ground plane. For a perfectly conducting ground plane, s is equal to twice the antenna height above the ground. The characteristic impedance Z_0 can then be computed from equation (18), assuming the perfectly conducting ground and an antenna diameter of 4 in. The results are compared with the measured data in table I. It is noted that the computed values of Z_0 are 1.5 to 1.8 times greater than the measured values of Z. The

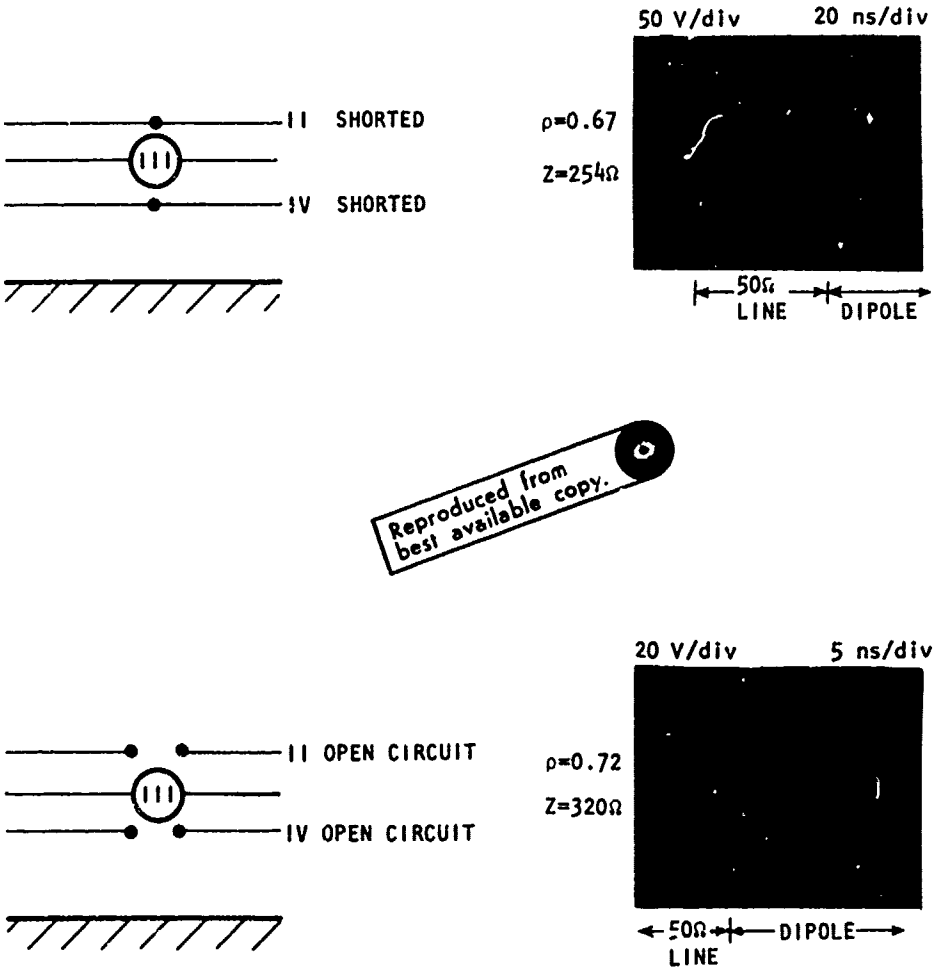


Figure 18. Time-domain reflectometry. The effect of adjacent elements on the measured impedance of the dipole antenna.

trends are corrected, however, as evidenced by the comparison of relative impedance changes as a function of change in antenna height for both the computed and measured values given in table 1b. The correlation of results is good, adding to confidence in the TDR measurements.

5.2 Determination of Mutual Coupling Losses

To study the effects of mutual coupling, the center antenna III is chosen as a typical element in the broadside array and the network representation is used to obtain the current and the electric field radiated by antenna III in the presence of adjacent elements II and IV. The mutual coupling losses introduced by the adjacent array elements can then be determined by comparison with performance of antenna III when all other antennas are removed. Measurements of impedance for antenna III were also taken with all five elements present in the array. No difference in impedance was observed when elements I and V were removed; therefore, only the effect of adjacent elements on the performance of an antenna in the array is considered.

Figure 18 shows the results of TDR measurements for the input impedance of antenna III in the presence of shorted and open circuited adjacent elements. In the open circuit condition,

Table Ia. Comparison of measured and computed input impedance for a dipole antenna above a ground plane

Antenna Number	Antenna Height (Meters)	Computed Z_0 (ohms)	TDR Measured Z (ohms)
I	3.96	606	366
III	2.44	548	320
V	0.91	430	284

Table Ib. Comparison between computed and measured relative impedance change as a function of change in antenna height

Computed	Measured
Z(I)/Z(III) = 606/548 = 1.11	366/320 = 1.14
Z(III)/Z(V) = 548/430 = 1.27	320/284 = 1.13
Z(I)/Z(V) = 606/430 = 1.41	366/284 = 1.29

the input impedance is the same as in the previous case where no other elements were present. This agrees with discussions of mutual coupling in antenna texts, namely that open-circuited elements should not effect the performance of active elements in an array. In the short-circuit condition, the impedance changes from 320 to 254 Ω indicating that the adjacent elements have a significant effect on the performance of antenna III. The equivalent circuit for this condition is shown in figure 19, where e_1 represents the voltage at the terminals of antenna III, and Z_{11} and Z_{22} represent the self-impedances of antenna III and the adjacent elements, respectively. The mutual impedance is represented by Z_{12}. The associated network relations are given by equations (19) and (20).

$$e_1 = I_1 Z_{11} - I_2 Z_{12} \tag{19}$$

$$0 = - I_1 Z_{12} + I_2 Z_{22}. \tag{20}$$

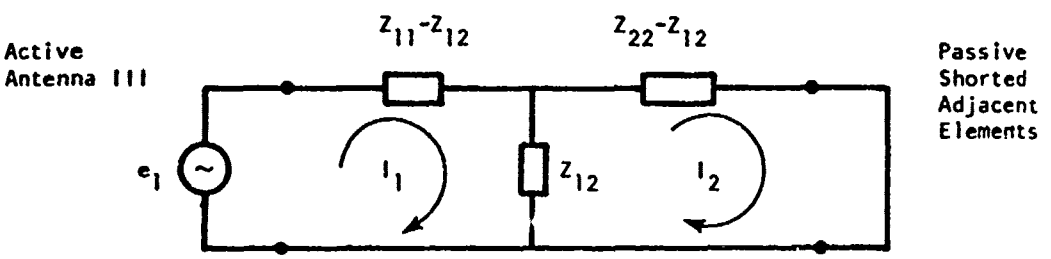


Figure 19. Network representation of mutual impedance.

The mutual impedance is determined experimentally by the following procedures:[2]

(1) The self-impedance Z_{11} of antenna III is measured with all other elements removed.

(2) The impedance Z_1 into antenna III is measured with shorted adjacent elements II and IV.

The mutual impedance is then computed from:

$$Z_{12} = \sqrt{Z_{11}\,(Z_{11} - Z_1)}. \tag{21}$$

Equation (21) assumes adjacent shorted elements with $Z_{11} = Z_{22}$ for identical antenna elements. One obtains Z_{11} and Z_1 from figures 17 and 18, respectively, and the mutual impedance Z_{12} can be computed from equation (21):

$$Z_{12} = \sqrt{320\,(320 - 254)} = 146\,\Omega \tag{22}$$

Next, determine the voltage e_1 across the biconic section of antenna III as follows. The generator voltage V_g is 30 kV at the pulser. This in turn is transmitted through a 100-Ω line to the input at the biconic section of the antenna. At this point there is a mismatch in impedance with an associated reflection coefficient Γ:

$$\Gamma = \frac{Z - 100}{Z + 100} \tag{23}$$

where $Z = 320\ \Omega$, the self-impedance of antenna III. Compute e_i by:

$$e_1 = (1 - \Gamma)V_g \tag{24}$$

In this case, $\Gamma = 0.52$ and $e_1 = 14.4$ kV. Sufficient data are available to compute the currents in equations (19) and (20). The computation results in $I_1 = 56.83$ amperes (A), and $I_2 = -25.9$ A. Therefore, in the short-circuited adjacent element condition, antenna III induces a net current of -25.9 A in the adjacent elements. This current in turn radiates an opposing field to the field of the active element III and causes a decrease in resultant field strength.

A formula for computing the peak free space electric-field strength at r on the centerline of a bicone-fed dipole antenna is:[3]

$$E_0 = \frac{60\,v}{Z\,r} = \frac{60\,I}{r}, \tag{25}$$

---

[2]Hansen, R. C. Microwave Scanning Antennas, Volume II Array Theory and Practice. Academic Press, N.Y. 1966, pp. 157-160.

[3]Schelkunoff, S. A., Friis, H. T., Antennas, Theory and Practice. John Wiley and Sons, Inc., N.Y. 1952, p. 106.

where v is the terminal voltage and Z is the self-impedance of the antenna. In our case, $v = e_1 = 14.4$ kV, $Z = 320\ \Omega$, and r = 12.2m. The net antenna current I is equal to 45A in the absence of other antenna elements. This corresponds to a free-field strength of $E_0 = 222$ V/m for antenna III. In the lossy case, where the adjacent short-circuited elements reduce the net current to I = 56.83 - 25.9 = 30.93A the corresponding field strength is $E_0 = 152$ V/m. (In the strict sense, the subtraction should include retarded time effects. However, the element spacing is so close that a direct subtraction is justified.) Consequently, mutual coupling has reduced the efficiency of antenna III to 69% of its original output.

The mutual coupling studies have shown that significant losses can arise from parasitic adjacent elements in an array. Therefore, design considerations should include these effects. The arguments presented in this section have been based on the impedance measurements and the network representations of mutual coupling. From these considerations, we obtained the net current and field strengths required to obtain the decrease in efficiency of a radiating element in the presence of adjacent antennas. In the following section, the efficiency of the arrays studied in this report is discussed from the standpoint of measured fields. Thus, one has the results of two approaches to estimating array efficiency: one approach dependent upon knowledge of impedances and voltages in the array (and independent of the radiated fields), and the other approach dependent upon knowledge of the radiated fields (and independent of the impedances and voltages in the array).

6. EFFICIENCY FACTOR OF THE ARRAY MODELS

Two mechanisms for degradation of performance have been identified which introduce limitations in the dipole technique for EMP simulation. Neglecting other losses, the physical size of the array determines a minimum range where the waveshape is not degraded by the arrival time differences from extreme elements. The array is a distributed source for practical ranges; therefore, the field strengths do not reach the ideal N times the single-element output level, where N is the number of antennas in the array.

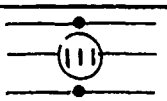
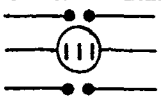
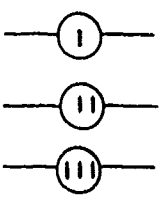
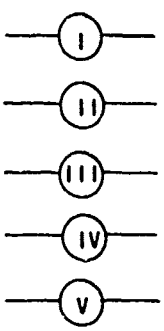
Define a lossless efficiency factor (E.F.) that provides a measure of how much the distributed nature of the array affects the output, as compared with the output of a point source having N times the single-array element strength. The H_{xT} component is used as a reference field for the computations.

$$\text{LOSSLESS E. F.} = \left(\frac{1}{N}\right)\left(\frac{\text{computed } H_{xT} \text{ for lossless array}}{\text{computed } H_{xT} \text{ for single element}}\right) \times 100\% \qquad (26)$$

The E.F. factor approaches 100% at ranges where the array approximates a point source. Table II shows computed values of the lossless E.F. for the array configurations studied in this report. The efficiency computed from H_{xT} is, in general, less than that obtained from the free-field output, as evidenced by the results shown for the five-element array in figure 10. For that case, the free-field efficiency approached 100%, whereas the use of H_{xT} in equation (26) has resulted in an efficiency factor of 76%.

Additional losses are introduced by mutual coupling effects. These losses are included in a second E.F. which is referenced to the measured H_{xT} component, and which includes any other real losses present in the array.

Table II. The array efficiency factor

ANTENNA CONFIGURATION	REFERENCE FIELDS (A/m) LOSSLESS H_{xT}	REFERENCE FIELDS (A/m) MEASURED H_{xT}	EFFICIENCY FACTOR LOSSLESS E.F.	EFFICIENCY FACTOR MEASURED E.F.
	0.32	0.34		
	0.33	0.33		
	0.33	0.22	100%	67%
	0.33	0.29	100%	88%
	0.95	0.85	99%	84%
	1.22	0.97	76%	59%

$$\text{MEASURED E. F.} = \left(\frac{1}{N}\right)\left(\frac{\text{measured array } H_{xT}}{\text{measured single element } H_{xT}}\right) \times 100\% \qquad (27)$$

Results of the computations are given in table II.

For antenna III with short-circuited adjacent elements, the measured E.F. is 67%. This agrees closely with the 69% efficiency predicted by the mutual coupling results. In the open

circuit adjacent element condition, the measured E.F. is 88%. This indicates that losses are introduced which were not apparent in the impedance measurements. The early time fields from the collinear array can be considered as a three-element broadside array. The measured E.F. is 84% for this condition. By comparison, the five-element broadside array measured efficiency is 59%. This indicates that increasing the number of elements in order to increase field strength has a practical limit, beyond which little is gained by adding elements.

7. CONCLUSIONS

This report summarizes the results of studies conducted at the HDL Electromagnetic Effects Laboratory on nuclear electromagnetic pulse simulation by dipole antenna array techniques. It is evident from these studies that the aperture size and range of operation are important factors that must be taken into consideration in the dipole array design. The dimensions of interest are the path length difference between extreme elements in the array and the point of observation in the test area. The transit-time differences must be at least smaller than the rise time of the single-element free space pulse to prevent waveshape degradation. Large apertures in either or both the electric and magnetic directions may cause this degradation.

Losses from mutual coupling must also be considered in design procedures. The method presented in this report can be used to estimate these losses by taking impedance measurements on reduced scale models, or possibly on full size models of large antenna elements. The efficiencies computed for the array configurations studied in this report should be considered as representative examples of the correlation between the various impedance, current, voltage, and field parameters for dipole antenna arrays. The efficiency factors indicate that optimal arrays should have as few antenna elements as possible to reduce losses introduced by mutual coupling and by distributed source effects. The theoretical methods and the computer programs developed during this study have been supported by experimental results, and can be used to predict the output of such arrays.